ANALYSING FLOW IN ROCKS BY COMBINED POSITRON EMISSION TOMOGRAPHY AND COMPUTED TOMOGRAPHY IMAGING

Yibing Hu[1], Ryan. T. Armstrong[1], Tzong-tyng Hung[2], Brendan Lee[2], Igor Shikhov[1], and Peyman Mostaghimi[1]

[1]School of Petroleum Engineering, The University of New South Wales, NSW 2052, Australia

[2]Biological Resources Imaging Laboratory, Mark Wainwright Analytical Centre, The University of New South Wales, NSW 2052, Australia

This paper was prepared for presentation at the International Symposium of the Society of Core Analysts held in Vienna, Austria, 27 August – 1 September 2017.

ABSTRACT

Combined Positron Emission Tomography (PET) and micro-Computed Tomography (micro-CT) provides an unprecedented imaging method to visualise and study fluid flow in porous media by continuous monitoring of tracer labelled fluid distribution in the pore space. We employ this method for understanding complex displacement processes in core samples to evaluate and visualise fluid flow. A flow cell to hold core samples and distribute the fluid has been designed and mounted within the PET-CT scanner. Each sample is imaged with micro-CT scanner and then moved into the PET chamber. Reservoir fluid labelled by radioisotope, [^{18}F]-FluoroDeoxyGlucose (18F-FDG) is injected by a syringe pump with pre-set rate and then continuous imaging is conducted by PET. The ^{18}F-FDG decays and emits positrons whose annihilation produces gamma rays. Image reconstruction and segmentation is applied for visualisation and simulation. The spatial fluid saturation is displayed by processing normalized radiation intensity values and the detection of the labelled flow phase. The tracer distribution illustrates the fluid pathways. The 3D flow displacement procedure is displayed, and the flow mechanisms are studied by analysing flow and core structure data acquired from the PET and CT scanners. The developed imaging method provides a unique opportunity to determine the pathway of fluid flow in porous media and offers detailed information on the fluid transport processes.

INTRODUCTION

This work reports a qualitative study on a fluid displacement experiment using combined PET and micro-CT imaging techniques. Micro-CT is a powerful tool for studying reservoir rock properties in 3D [1] and is recently used for visualising dynamic flow in rocks [2]. Schembre and Kovscek [3] measured dynamic relative permeability from CT monitored spontaneous imbibition experiments on Berea sandstone and diatomite cores. They used CT imaging to collect the saturation profile for their calculation and the method showed good reliability in measurement of relative permeability curve. Berg et al. [2] studied multiphase flow drainage and imbibition in sandstones and limestones using fast dynamic micro-CT. They imaged real-time pore-scale fluid displacement, and observed drainage Haines jump events and imbibition snap-off events. However, micro-CT dynamic imaging has the drawback of limited temporal resolution and sample size.

An alternative method to visualise dynamic flow processes in porous media is using PET. High-resolution PET combined with micro-CT can be applied for the qualitative and quantitative

study of flow and to image the fluid distribution and front progress in 4D. Ferno et al. [4] applied the combined PET and CT imaging of the saturation processes in sandstones and chalks for visualisation of fluid displacement and gas injection within the core sample. They used ^{22}Na ($t_{1/2}\approx2.6$ years) and calculated the spatial fluid saturation based on the CT number and time-averaged radiation intensity ratio from PET. The activity profile and fluid front were acquired and plotted against imaging time and core length, thus comparing the signal-to-noise ratio of PET and CT. Pini et al. [5] investigated the small-scale heterogeneity of Berea sandstones by implementing micro-CT and PET scanning. They described spatial and temporal progression of $NaHCO_3$ solution labelled with ^{11}C. They studied the radioactivity advection-dispersion transport by analysing tracer activity and decay by measuring residence-time and tracer mass balance. The comparative study of concentration profiles as a function of time or distance from the tracer transport imaging and 1D "streamtube" model for tracer spread showed similarity in the tracer plume movement and. Zahasky and Benson [6] used micro-CT and PET to verify the fluid saturation in a Berea core. They calculated the flow saturation, estimated the average capillary pressure, and derived voxel permeability equation.

This work reports results from a qualitative study on fluid displacement experiments using combined PET and micro-CT imaging techniques. It investigates combined PET and micro-CT imaging of fluid movement labelled by the radioactive tracer ^{18}F-FDG. The results of PET imaging are compared with micro-scale numerical simulation for flow distribution and permeability estimation.

METHODOLOGY

PET Imaging

The Inveon MicroPET-CT scanner (Siemens) used in this work is capable of providing three dimensional micro-CT and micro-PET images of samples. The system has a variable focus X-ray source and a detector of 2048×3096 pixels. The Inveon micro-PET is equipped with an LSO detector for fast scintillation decay time, highlight output and effective atomic number. The micro-CT imaging resolution is 0.425 mm and the PET camera resolution is 0.776 mm. The PET camera captures positron-emitting radioisotope radiation and generates the dataset of the distribution of radioactivity. ^{18}F –FDG is used in this work as it has proved to be effective for the imaging of fractured reservoir rocks [7,8].

The radioisotope is diluted by the injection fluid, and injected into the matrix by an NE-1050 syringe pump. The decaying isotope will emit low energy positrons (in MeV range) which can travel in surrounding media a distance in the order of millimetres. The positive charge of the positron can attract an electron and lead to annihilation, generating two photons with 511 keV of energy. The photons are emitted in the form of gamma rays in opposite directions (180^0 to each other) and detected in coincidence. The detectors are made of lutetium oxyorthosilicate crystals and arranged in a circle. The detector can define their line of response (LOR), thereby reconstructing the tomographic image of isotope distribution from a dataset of LORs. The reconstructed 2D images can be stacked to make 3D images and coupled with temporal information to generate 4D dataset.

Experiment Design

As Figure 1 shows, sample A is made of Sigma-Aldrich borosilicate glass beads of 6 mm diameter packed in a polycarbonate tube of 25 mm in diameter. Sample B is an artificially fractured Bentheimer sandstone core of 25 mm in diameter and 50 mm in length. Sample C is a Bentheimer sandstone core of 25 mm in diameter and 55 mm in length. Porosity of each sample is calculated on segmented micro-CT images using software Mango and the images are

pre-processed by Unsharp Mask, Neighbourhood Filter and Converging Active Contours Segmentation [9]. The samples are dried in the vacuum drying oven and sealed in the flow cells. The flow cell is made of polycarbonate tubes and sealed with araldite plug. It is designed and duplicated to contain the samples, distribute fluid from the syringe pump through the core into the collection vessel and test the flowing characteristics. The connection PEEK (polyether ether ketone) tubing is fitted with soft silicon tubing and the fitting points are sealed with thermoplastic to prevent leakage. The flow cell connected to the collection vessel with outlet tubing is placed in the scanner for the initial micro-CT scan. While the micro-CT scan is being performed, we prepare the radioactive substance behind the L-Block (Lead shields). 30-60 MBq of ^{18}F-FDG was diluted in 50 ml water and drawn into a syringe. At the rear of the instrument where the micro-PET imaging component resides, the syringe is loaded on the pre-programmed pump and attached to the inlet tubing. The PET image is acquired for 30-70 minutes.

Figure 1. (left) sample A: glass beads pack (37 % in porosity); (middle) sample B: fractured sandstone (18.44 % in porosity); (right) sample C: sandstone (16.28 % in porosity).

Permeability Calculation

The permeability of the three samples is estimated using two methods. For sample A, the permeability is related to packing mechanism, particle size and compactness of packing. For granular packing, the permeability can be estimated by the Kozeny-Carman Equation [10,11]:

$$k = \frac{d^2 \varepsilon^3}{36 K_0 \tau^2 (1-\varepsilon)^2} \qquad (1)$$

where d is the average diameter of the glass spheres, ε is the total porosity, $K_0\tau^2$ is the Kozeny's coefficient and can be assumed as 4.2-5.0 for granular packs with porosity range from 0.36 to 0.4 (this sample is 0.37) [11].

For sample B and C, Finite Element Method (FEM) was employed for flow simulation and rock permeability calculation via the GeoDict package [12]. To calculate absolute permeability of the rock samples, we use the Left Identity Right (LIR) solver for the Navier-Stokes equations with periodic boundary condition [13]. To calculate permeability of the entire core samples, we take subsections with a range of porosity values from the micro-CT images and fit the porosity and simulated permeability value to a linear relationship [14]. The absolute permeability from the simulation is used to plot a 3D map of voxel permeability to demonstrate the heterogeneity of the core. The permeability is influenced by the image resolution and number of voxels capturing flow pathways [15]. The samples considered in this paper have high permeability and large pore sizes that are well captured by the micro-CT image. For low-permeability samples, in range of mD and below, image registration and calibration can be employed to improve the quality of images and resolve small pore sizes [15].

Voxel Permeability 3D map

Using the PET imaging results, we are able to visualise flow distribution and migration in the cores and combine them with micro-CT images to demonstrate the heterogeneity of the sample. Voxel permeability map is created by averaging the properties from high resolution CT images to make PET voxel sized subsection and coupling it with PET imaging results. In each voxel of the PET image, the permeability can be calculated on the micro-CT images as [6]:

$$k_i = \phi_i \frac{1}{\overline{P_c}^2}\left[\sigma_{w/nw}\cos\theta_{w/nw} J(\mathrm{S}_{w,i})\right]^2 \qquad (2)$$

where k_i is the voxel permeability, ϕ_i is the voxel porosity (from CT images), $\overline{P}_c$ is the average capillary pressure of the slice, $\sigma_{w/nw}$ is the surface tension, $\cos\theta_{w/nw}$ is the contact angle and $J(\mathrm{S}_{w,i})$ is the J-Leverett function. The J - Leverett function can be derived as [6]:

$$J(\mathrm{S}_{w,i}) = \frac{P_c(\mathrm{S}_{w,i})}{\sigma_{w/nw}\cos\theta_{w/nw}}\sqrt{\frac{k_c}{\phi_c}} \qquad (3)$$

where $P_c(\mathrm{S}_{w,i})$ is the voxel capillary pressure, k_c is the sample permeability and ϕ_c is the sample porosity.

We can derive, from the above equations, the voxel permeability for the PET and micro-CT images:

$$k_i = \phi_i \frac{1}{\overline{P_c}^2}\left[P_c(\mathrm{S}_{w,i})\sqrt{\frac{k_c}{\phi_c}}\right]^2 \qquad (4)$$

The capillary pressure curve is simulated on the micro-CT images using the Pore Morphology Method [16]. The distribution of the fluid is determined by estimating the pore space accessible to the non-wetting phase (NWP) using Young- Laplace equation for a spherical interface. Each sphere works as a probe to make new pore space accessible and the probe locations are included in the NWP portion of the total space. Voxel saturation is obtained by normalizing the intensity value of the PET images. For each voxel of the PET, we calculate voxel porosity based on the micro-CT images and by combining it with the capillary pressure value, we obtain the permeability using Equation 4.

RESULTS

Fluid Saturation Process

The experiment parameters are included in the table below:

Table 1. PET experiment parameters

Sample	Flow Rate (ml/min)	Injected Volume (ml)	Pore Volume (ml)	Dose (Mbq)
Glass beads (A)	0.5	15	11.4	33.7
Fractured sandstone (B)	0.1	7	6.2	40.2
Sandstone (C)	0.1	6	5.6	60.0

Glass Beads Pack

Figure 2 is the CT image from PET-CT scan and it shows the packing of the glass beads. The saturation process (Figure 3) of the sample shows gravity dominated flow in large pores as the fluid fills the sample from bottom to top with a relatively even surface. Another phenomenon from the comparison between PET and CT images is that the radioactivity may exaggerate the saturation of fluid, as one can observe from the PET images that the concave areas are larger than the individual beads.

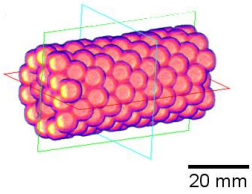

Figure 2. PET-CT image of the sample A.

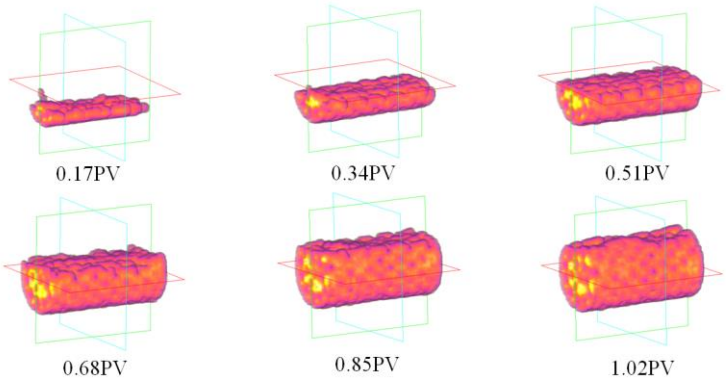

Figure 3. PET images of fluid saturation in sample A.

Fractured Sandstone

Figure 4 shows the PET-CT image of the sample. A low porosity region can be observed in the middle of PET-CT image, which could be the micro-pore region below the resolution.

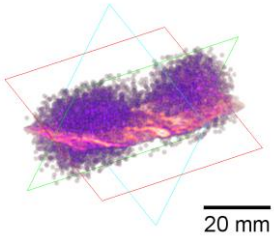

Figure 4. PET-CT image of fractured sample B.

Figure 5 shows the saturation process with PET imaging. Gravity affected flow can be observed before 0.6 PV as the activity propagates below the fracture. The fluid fills the bottom half of the sample in a capillary dominated flow pattern. At 0.6 PV, the fluid saturated zone starts to grow from both ends to meet in the middle where the low porosity zone.

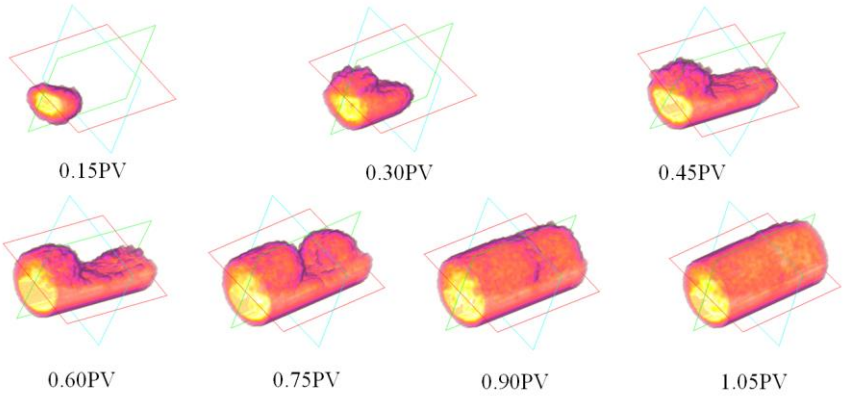

Figure 5. PET images of fluid saturation in sample B.

Sandstone

Figure 6 is the PET-CT of sample C. Figure 7 shows a diffusion flow phenomenon at the front as the flow is dominated by capillary force. The flow at 0.17 PV forms a smaller cylindrical fluid distribution and then diffuses to fill the entire section. After 0.51 PV, individual boluses can be detected at the rear of the saturated zone, which shows a higher flow rate than the uniform front.

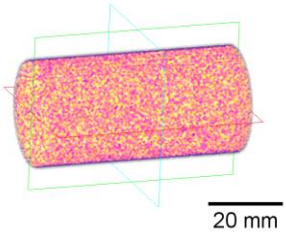

Figure 6. PET-CT image of sample C.

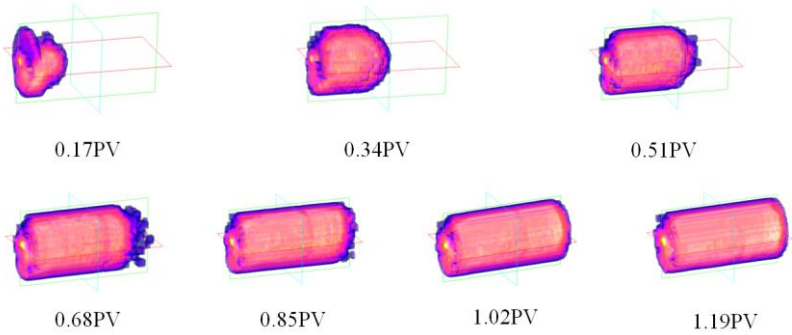

Figure 7. PET images of fluid saturation in sample C.

Permeability

Absolute permeability in the injection direction of the three samples measured with the methods described above is listed in the table below:

Table 2. Absolute permeability measurements

Sample	Permeability (mD)	Method	Porosity
Glass beads (A)	2.58×10^5	Kozeny-Carman	37%
Fractured sandstone (B)	4565	FEM simulation	18.44%
Sandstone (C)	1236	FEM simulation	16.28%

Figure 8 presents the FEM simulation results of the fractured sandstone. The velocity field of the artificial fracture shows similarity with the PET flow imaging with regard to the low flow rate (porosity) zone. The pressure field shows the pressure drop from injection end to the collection end. Contrary to the simulation results, the PET flow image shows that the fluid accumulates at the rear of the sample and builds pressure before entering the collection tube.

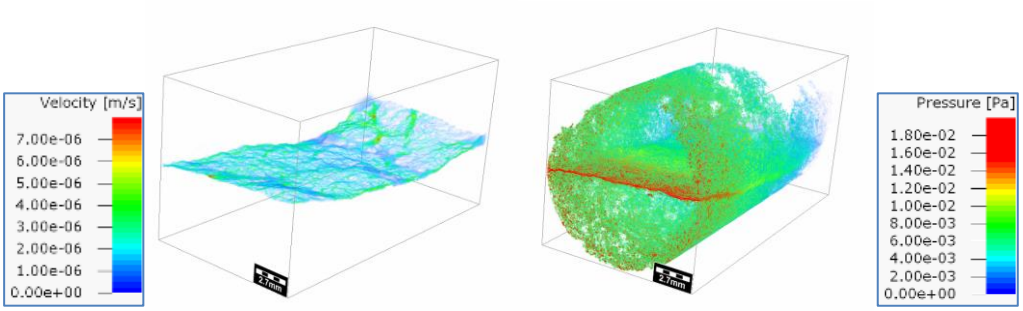

Figure 8. (left) velocity field of artificial fracture; (right) pressure field of fractured sandstone.

Voxel 3D map

Figure 9 is the slice averaged voxel porosity and saturation map of sample C. The voxel porosity map is created by resampling the micro-CT image to the resolution of the PET image. The voxel saturation map is generated by using the method explained for voxel saturation in Equation 4. Low values are on the edge and it can be the result of limited time for diffusion.

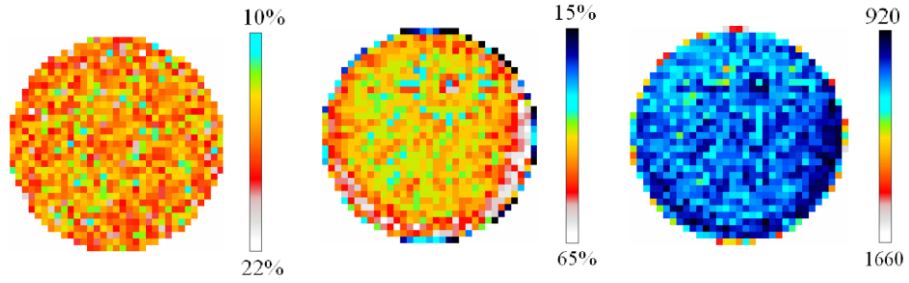

Figure 9. (left) voxel porosity map, highlighting the pore space heterogeneity in the direction parallel to the axis; (middle) voxel saturation map, lowest values on the boundary (possibly caused by short diffusion time); (right) voxel permeability map (mD).

The voxel permeability map (Figure 9) is the result of applying Equation 4 on the porosity and saturation maps and averaging. The voxel permeability ranges from 920 mD to 1660 mD and Figure 9 shows a relatively low permeability region on the bottom half of the sample.

CONCLUSION AND FUTURE WORKS

This work combines PET imaging and micro-CT imaging to describe flow in porous media. The qualitative study by high resolution PET imaging visualises the fluid distribution and propagation through different cores. Numerical simulations were performed to obtain permeability maps. Below conclusions can be drawn from this study:

1. The combination of high resolution PET imaging and micro-CT imaging shows great potential in study of flow in porous media.

2. PET imaging is capable of capturing the saturation process and 3D spatial fluid distribution in cores. The dominating flow displacement pattern can be observed from the dynamic PET images.

3. Voxel-averaged maps based on high resolution micro-CT and PET dynamic imaging exhibit the structural heterogeneity of the samples.

In the future studies, the voxel-averaged map can be involved in the larger scale simulators to simulate the front progression of the injection phase. Vertical set up can help to eliminate the gravity affection and this needs further design of the apparatus.

Reference

1. Mostaghimi, P., Armstrong, R.T., Gerami, A., Warkaini, M.E., Ramandi, H.L. and Pinczewski, V., "Micro-CT imaging and microfluidics for understanding flow in coal seam reservoirs," In *International Symposium of the Society of Core Analysts, Newfoundland, Canada*. (2015). SCA2015-051.
2. Berg, S., Armstrong, R., Ott, H., Georgiadis, A., Klapp, S. A., Schwing, A., Neiteler, R., Brussee, N., Makurat, A., Leu, L. and Enzmann, F., "Multiphase flow in porous rock imaged under dynamic flow conditions with fast X-ray computed microtomography," *Petrophysics*, (2014)**55,** 4, 304–312.
3. Schembre, J. M., & Kovscek, a. R., "Direct Measurement of Dynamic Relative Permeability from CT Monitored Spontaneous Imbibition Experiments," *Proceedings of SPE Annual Technical Conference and Exhibition.* (2001). SPE-71484
4. Ferno, M., Gauteplass, J., Hauge, L. P., Abell, G. E., Adamsen, T. C. H., & Graue, A., "Combined positron emission tomography and computed tomography to visualise and quantify fluid flow in sedimentary rocks," *Water Resources Research*, (2015) **51,** 9, 7811–7819.
5. Pini, R., Vandehey, N. T., Druhan, J., & Neil, J. P. O., "Quantifying solute spreading and mixing in reservoir rocks using 3D PET imaging," *Journal of Fluid Mechanics*, (2016) **796,** 558–587.
6. Zahasky, C., & Benson, S. M., "Phase Saturation Validation and Tracer Transport Quantification Using Micropet in a Heterogeneous Sandstone Core," *the International Symposium of the Society of Core Analysts, Snowmass, Colorado, USA.* (2016), SCA2016-028.
7. Mau, M., Dusterhoft, R., Rickman, R., Gibson, R., Energy, H., Buffler, A., Heerden, M. Van., "Dynamic Imaging of Fluid Mobility in Low-Permeability Matrices Using Positron Emission Tomography," *Unconventional Resources Technology Conference, Denver, Colorado, USA.* (2013), 1–10.
8. Mau, M., Dusterhoft, R., Rickman, R., Gibson, R., Buffler, A., Heerden, M. Van, & Town, C., "Dynamic 3D Imaging of Fluid Mobility in Natural Fractures Using High-resolution Positron Emission Tomography," *International Petroleum Technology Conference, Doha, Qatar*. (2014), IPTC 17478.
9. Averdunk, H., "Mango User Guide," (2004,2005), Applied Mathematics, ANU.
10. Bear, J., *Dynamics of Fluids in Porous Media*, Dover Publications, Inc., New York, (1972), 112–167.
11. Dias, R. P., "Permeability analysis in bisized porous media : Wall effect between particles of different size," *Journal of Hydrology*, (2008) **349,** 470–474.
12. Jaganathan, S., Tafreshi, H. V., & Pourdeyhimi, B., "A Case Study of Realistic Two-Scale Modeling of Water Permeability in Fibrous Media," *Separation Science and Technology*, (2008) **43,** 8, 1901–1916.

13. Cheng, L., Wiegmann, A., Planas, B., "FlowDict2015 Reference," (2016).
14. Nelson, P.H., "Permeability-Porosity Relationships in Sedimentary Rocks," *The Log Analyst*. (1994), 38-62.
15. Mostaghimi, P., Armstrong, R.T., Gerami, A., Hu, Y., Jing, Y., Kamali, F., Liu, M., Liu, Z., Lu, X., Ramandi, H.L., Zamani, A., Zhang, Y., "Cleat-scale characterisation of coal: an overview," *Journal of Natural Gas Science and Engineering*, (2017) **39**, 143-160.
16. Hilpert, M. and Miller, C. "Pore-morphology-based simulation of drainage in totally wetting porous media," *Advances Water Resources*, (2001) **24**, 243 – 255.